Electronic Supplementary Information (ESI) for

Nitrogen-doped CeO_x Nanoparticles Modified Graphitic Carbon Nitride for Enhanced Photocatalytic Hydrogen Production

Jie Chen, Shaohua Shen*, Po Wu, Liejin Guo*

International Research Center for Renewable Energy, State Key Laboratory of Multiphase Flow in Power Engineering, Xian Jiaotong University, 28 Xianning West Road, Xi'an, Shaanxi 710049, China.

E-mail: shshen_xjtu@mail.xjtu.edu.cn (S. Shen), lj-guo@mail.xjtu.edu.cn (L. Guo)

Computational Methods

Based on first-principles density functional theory (DFT), calculations were performed using the ultrasoft pseudopotentials, together with the Perdew-Burke-Ernzerhof (PBE) exchange-correlation functional, implemented by CASTEP code. The electron wave function was expanded in plane waves up to a cutoff energy of 240 eV, and a medium (3×3×4) k-point was used for geometry optimization and following electronic structure calculations. The energy band tolerance is 1.0×10^{-5} eV.

Decay Kinetics Calculation Methods

In the present study, the value of the goodness-of-fit parameter (χ^2) calculated from the tri-exponential decay kinetics method[1,2] is much closer to 1, which indicates a good fit of the data.[3] Thus, the emission signals were analyzed by the tri-exponential decay kinetics method rather than other (mono-, bi-, or tetra-exponential) kinetics method. Equation (1) and Equation (2)[3] were applied to carry out the tri-exponential kinetic analysis and to calculate average lifetime τ_{avg}, respectively.

$$y = \sum \mathrm{A_i} e^{-(\frac{t}{\tau_i})} \quad (1)$$

$$\tau_{avg} = \frac{\sum \mathrm{A_i}\tau_\mathrm{i}^2}{\sum \mathrm{A_i}\tau_\mathrm{i}} \quad (2)$$

Table S1 The weight contents for all the elements (C, N, O, Ce) in g-C_3N_4 and Ce-CN-V photocatalysts.

Samples	C (wt%)	N (wt%)	O (wt%)	Ce (wt%)
g-C_3N_4	37.78	60.67	1.55	0.00
Ce-CN-1	37.29	60.04	1.72	0.95
Ce-CN-3	37.33	58.16	2.06	2.45
Ce-CN-5	36.42	56.91	2.45	4.22
Ce-CN-7	35.71	55.43	2.88	5.88
Ce-CN-10	34.36	53.67	3.45	8.52
Ce-CN-15	32.35	50.35	4.48	12.82

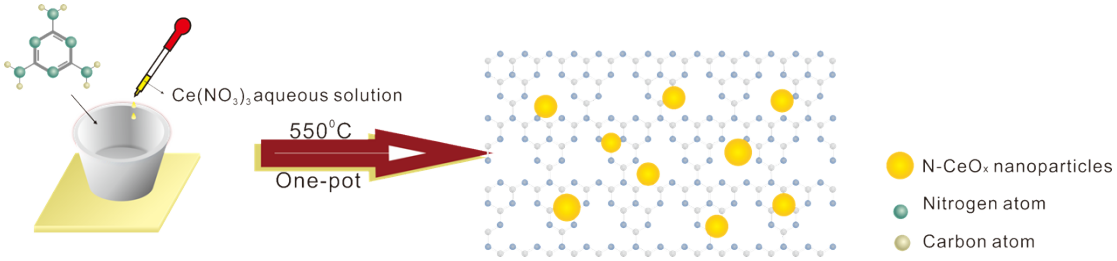

Fig. S1 Schematic illustration of the fabrication of the Ce-CN-V composite photocatalysts.

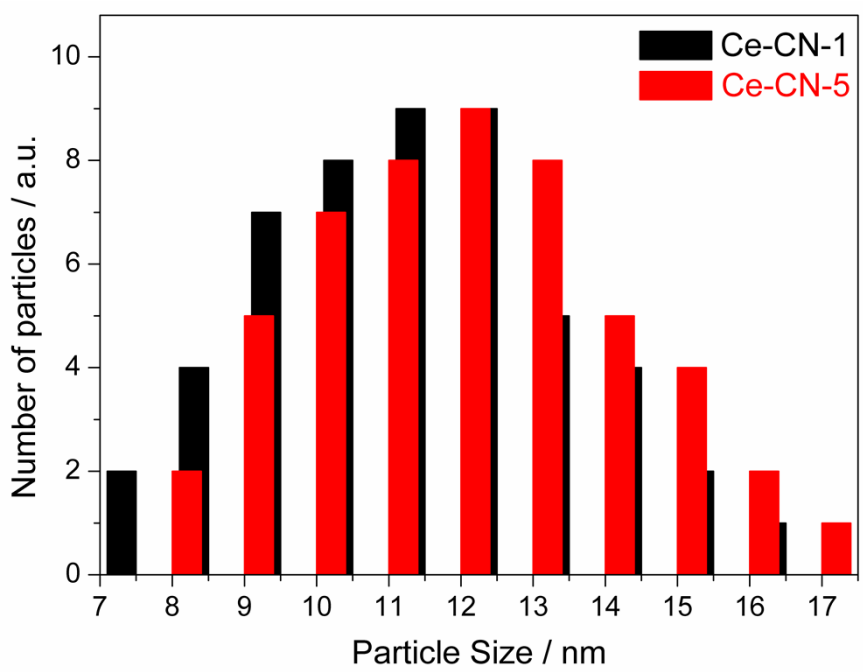

Fig. S2 The particle size distribution for Ce-CN-1 and Ce-CN-5 recorded by measuring more than 100 nanoparticles from the TEM images of the corresponding samples.

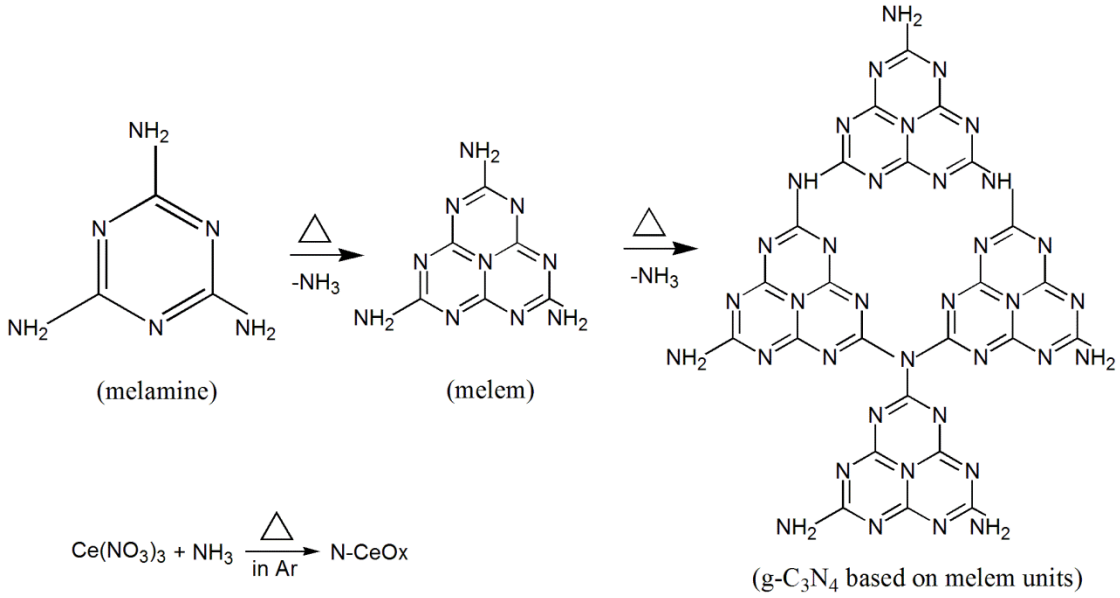

Fig. S3 The schematic illustration of the proposed formation process of N-CeO_x NPs on g-C_3N_4.

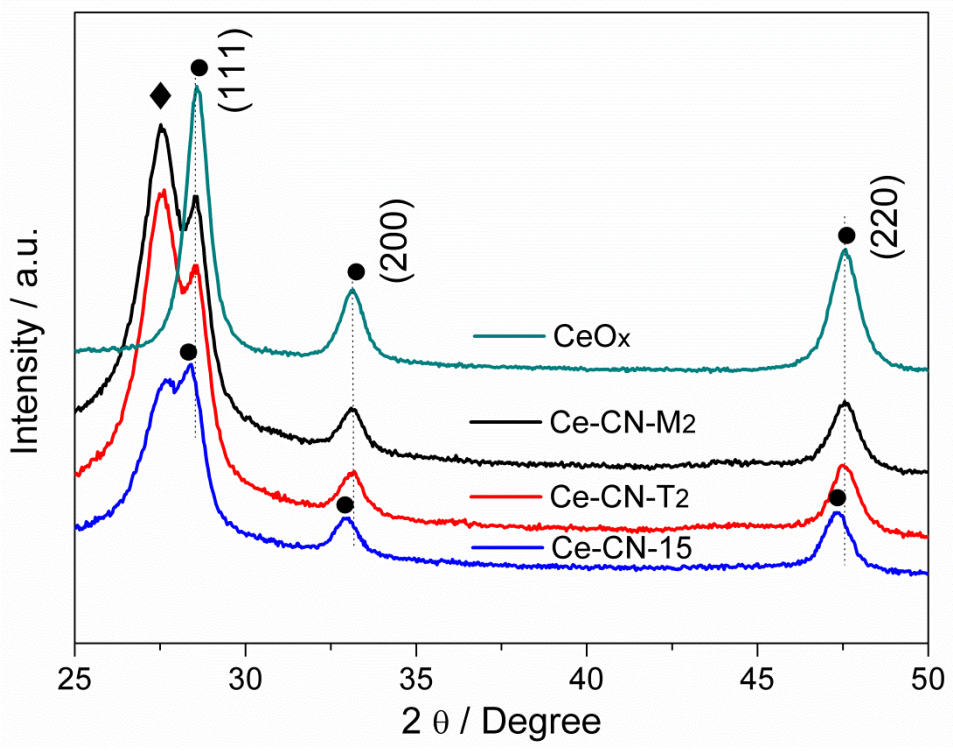

Fig. S4 The XRD patterns of Ce-CN-15, CeO_x and Ce-CN-M_2 and Ce-CN-T_2 photocatalysts.

As shown in Fig. S5, the increasing intensity of Ce 3d peaks should be due to the increased amount of Ce in Ce-CN-V photocatalysts. The XPS peaks of Ce 3d were undetectable for Ce-CN-V (V = 1, 3), possibly because of the detection limit of XPS instrument.

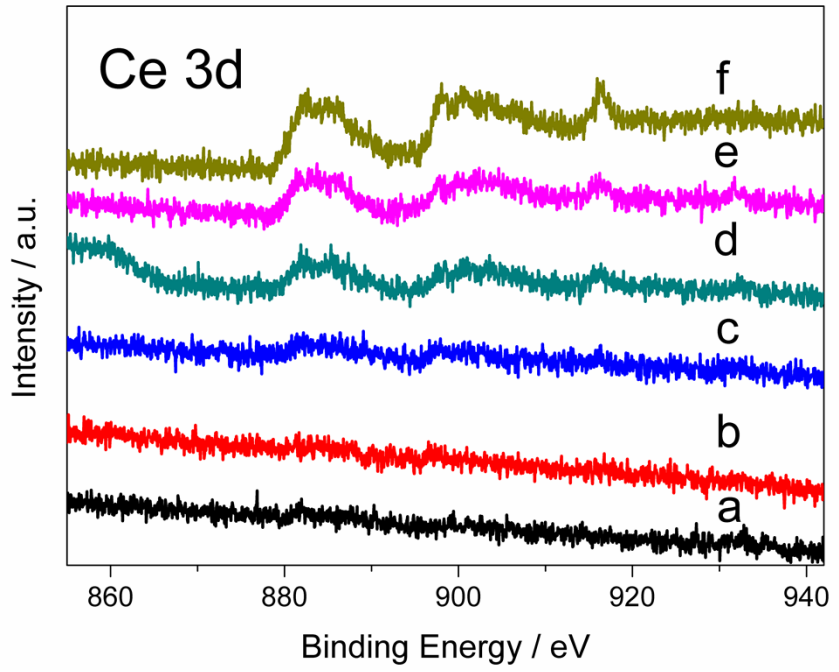

Fig. S5 Ce 3d XPS spectra of the Ce-CN-V photocatalysts prepared with V mL of 0.031 g/mL $Ce(NO_3)_3 \cdot 6H_2O$ aqueous solution: (a) V = 1, (b) V = 3, (c) V =5, (d) V = 7, (e) V = 10, (f) V = 15.

To further confirm the influence of N-doping on the electronic structure of CeO_x, DFT calculation[4] was carried out to demonstrate the narrowed band structure of CeO_x induced by nitrogen incorporation. As shown in Fig. S6, it was unambiguous to assign the absorption band of CeO_x to the transition from O 2p orbital (VB) to Ce 4f orbital (CB) as demonstrated from the calculated electronic band structures.[5,6] Compared to CeO_x, N-CeO_x has VB edge leveled up by 0.21 eV, due to the N-dopants introduced energy levels above the O 2p level,[7-9] while the CB edge was significantly lowered by 0.31 eV, thus resulting in the decreased bandgap energy.

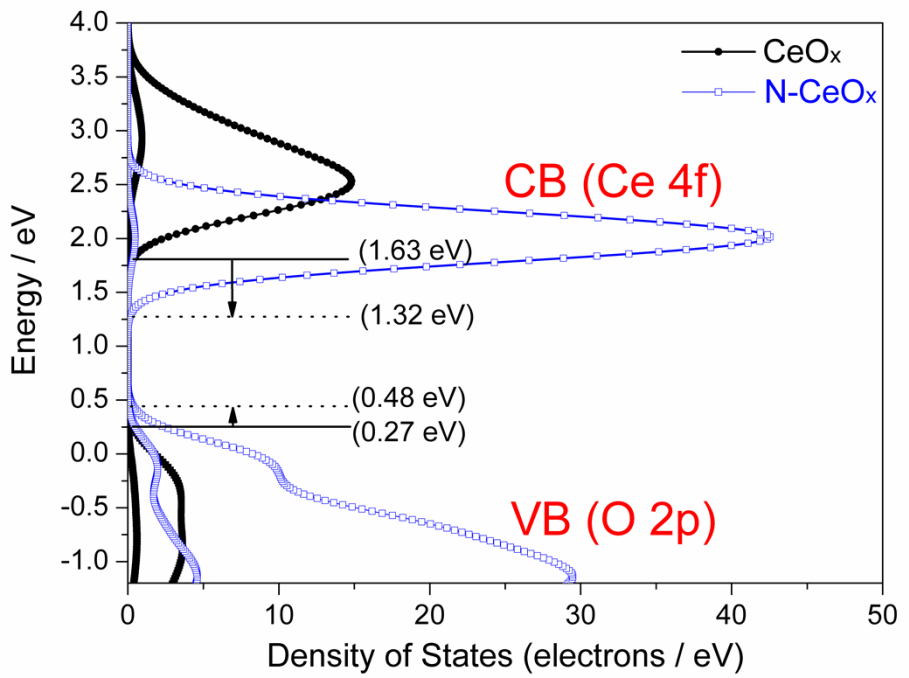

Fig. S6 DFT calculations of the densities of states of CeO_x and N-CeO_x. Solid line and dotted line represent the band positions for CeO_x and N-CeO_x respectively. CB: conduction band, VB: valence band.

As demonstrated from Fig. S7, the visible light absorption of Ce-CN-T and $CeO_x$was much weaker than that of Ce-CN-5, especially in the range of $\lambda > 500$ nm. This should be attributed to that nitrogen was not introduced into the lattice of CeO_x by the two-step method and the visible light absorption ability of CeO_x in Ce-CN-T was weaker than the N-CeO_x in Ce-CN-5.

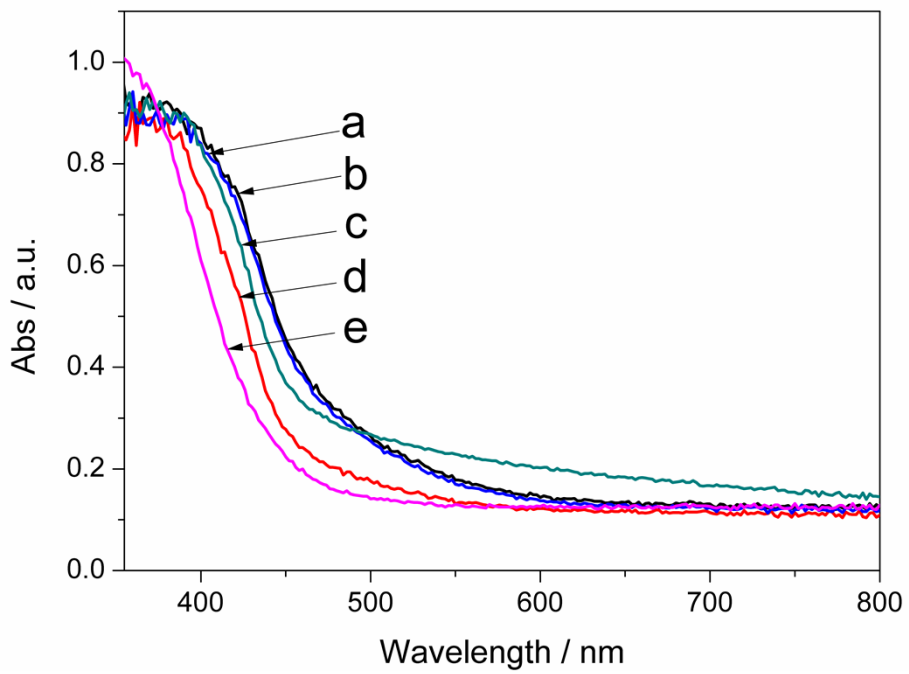

Fig. S7 UV-vis diffuse reflectance spectra of (a) pure g-C_3N_4, (b) Ce-CN-M, (c) Ce-CN-5, (d) Ce-CN-T, and (e) pure CeO_x photocatalysts.

As shown from Fig. S8, the N-CeO_x or CeO_x with different morphology and size were formed on the surface of g-C_3N_4 with different methods. As for Ce-CN-5 prepared by one-pot method, the N-CeO_x nanoparticles (NPs) are very small with a size range of 7-17 nm as shown in Fig. S8A, B. While for the Ce-CN-T prepared by the two-step method, the size of CeO_x turned out to be 40-50 nm (Fig. S8C,D), which was much larger than the N-CeO_x NPs in Ce-CN-5. Therefore, it can be deduced that the contact area of N-CeO_x/g-C_3N_4 heterojunction in Ce-CN-5 will be much larger than that of CeO_x/g-C_3N_4 heterojunction in Ce-CN-T, leading to more efficient charge carriers transfer between N-CeO_x and g-C_3N_4 in Ce-CN-5 than in Ce-CN-T. However, large CeO_x bulks are found in the Ce-CN-M sample prepared by the simple mechanical method (Fig. S8E). Besides, some of the CeO_x bulks are not in intense contact with the substrate g-C_3N_4, as shown from Fig. S8F, leading to bad formation of the CeO_x/g-C_3N_4 heterojunction and consequently poor charge carriers separation ability.

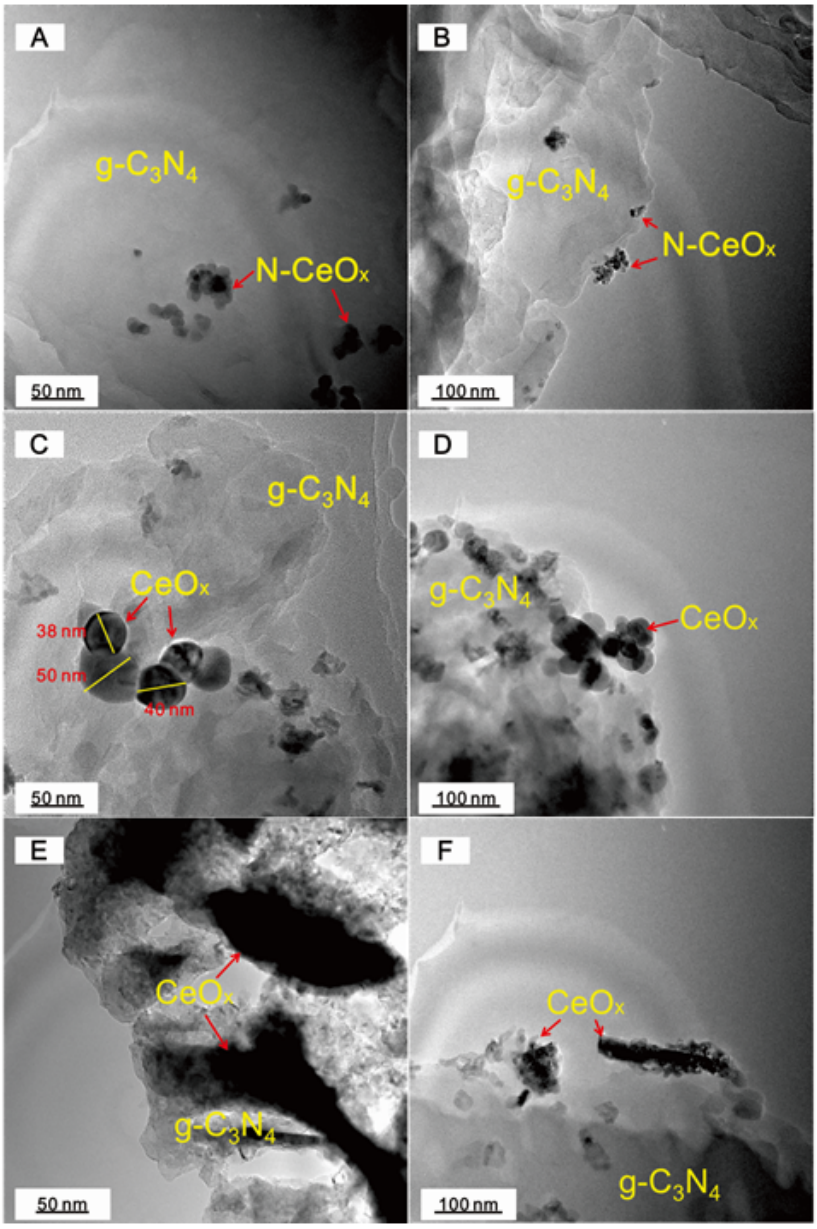

Fig. S8 TEM images of the photocatalysts prepared by different methods. (A), (B): Ce-CN-5 prepared by one-pot method, (C), (D): Ce-CN-T prepared by two-step method, (E), (F): Ce-CN-M prepared by mechanical method.

To prove the existence and function of Pt nanoparticles as hydrogen evolution sites, TEM images for Pt loaded Ce-CN-5 after the photocatalytic hydrogen production reaction were taken, as shown in Fig. S9. Fig. S9A shows the Pt loaded g-C_3N_4, Pt NPs with an average size of ca. 10 nm were formed on the surface of g-C_3N_4, acting as the hydrogen evolution sites. The shape and size of the Pt NPs are very much alike the reported morphology in the reference [10]and our previous report[11]. While for Pt loaded Ce-CN-5 in Fig. S9B, the 50 nm N-CeO_x NPs and 10 nm Pt NPs co-existed on g-C_3N_4.

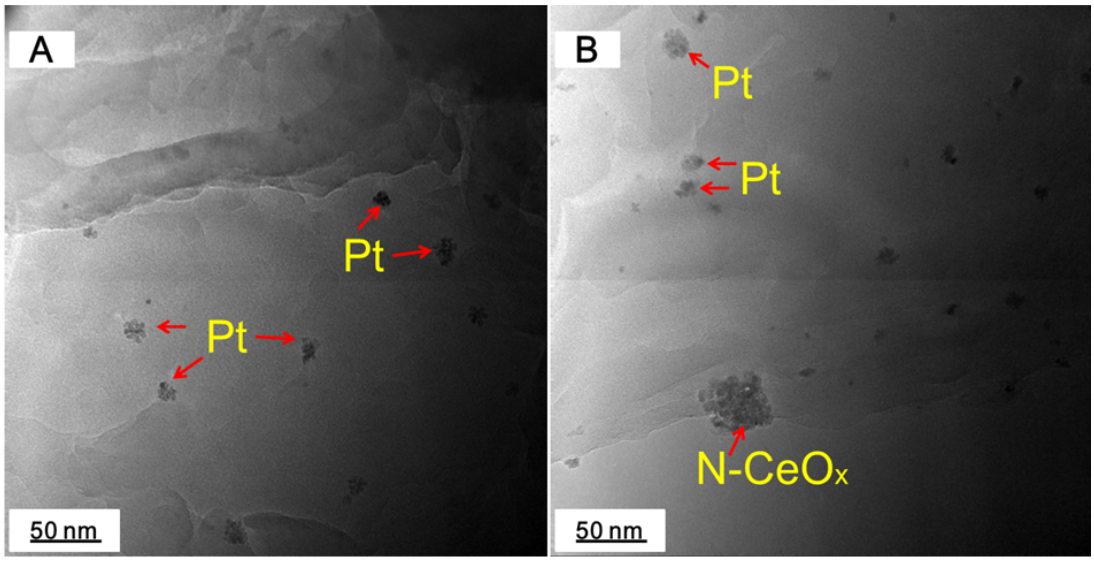

Fig. S9 TEM images of Pt loaded (A) g-C_3N_4 and (B) Ce-CN-5 after the photocatalytic hydrogen production reaction.

References

1 P. Niu, L. Zhang, G. Liu, H. M. Cheng, *Adv. Fun. Mater.*, 2012, **22**, 4763-4770.

2 S. Barman, M. Sadhukhan, *J. Mater. Chem.*, 2012, **22**, 21832-21837.

3 J. R. Lakowicz, Principles of fluorescence spectroscopy, *Springer*, 2009.

4 F. Goubin, X. Rocquefelte, M. H. Whangbo, Y. Montardi, R. Brec, S. Jobic, *J. Chem. Mater.*, 2004, **16**, 662-669.

5 W. Li, S. Xie, M. Li, X. Ouyang, G. Cui, X. Lu, Y. Tong, *J. Mater. Chem. A.*, 2013, **1**, 4190-4193.

6 R. Li, C. Fu, C. Q .Li, S. Yin, Y. Zhang, T. Sato, *J. Ceram. Soc. Jpn.*, 2010, **118**, 555-557.

7 R. Asahi, T. Morikawa, T. Ohwaki, K. Aoki, Y. Taga, *Science*, 2001, **293**, 269.

8 V. D. Di, G. Pacchioni, A. Selloni, S. Livraghi, E. Giamello, *J. Phys. Chem. B.*, 2005, **109**, 11414-11419.

9 Z. S. Lin, A. Orlov, R. M. Lambert, M. C. Payne, N *J. Phys. Chem. B.*, 2005, **109**, 20948-20952.

10 B. Chai, T. Y. Peng, J. Mao, K. Li, L. Zan. *Phys. Chem. Chem. Phys.*, 2012, **14**, 16745–16752.

11 J. Chen, S. Shen, P. Guo, P. Wu, L. Guo, *J. Mater. Chem. A.*, 2014, **2**, 4605-4612.